

Impact of high-resolution FWI in the Western Black Sea: Revealing overburden and reservoir complexity

Partha Routh¹, Ramesh Neelamani¹, Rongrong Lu¹, Spyros Lazaratos¹, Hendrik Braaksma¹, Steve Hughes², Rebecca Saltzer³, Jonathan Stewart³, Kiran Naidu¹, Heather Averill⁴, Vijay Gottumukkula², Peter Homonko², Joseph Reilly¹, and Damian Leslie⁵

Abstract

The Western Black Sea (WBS) is now an area of active petroleum exploration, and several seismic surveys have been acquired to support the ongoing activity. Seismic imaging in the WBS is challenging due to the presence of complex overburden, such as canyons, shallow gas channels, and complex shallow stratigraphy. Such overburden complexities create amplitude dimming and wipeouts in the images and cause structural distortions of the reservoir units. Conventional velocity model building and seismic migration methods are not optimal for addressing such challenges. Full-wavefield inversion (FWI) technology was applied to overcome the complex seismic-imaging challenges in the WBS and to support the exploration and development program. To date, a suite of FWI products has been used to identify shallow hazards, derisk prospects, optimize well placement, perform accurate resource estimation, and support development planning. Unlike traditional seismic migration, generated FWI products are not simply depictions of the seismic reflectivity but rather are high-resolution volumes of subsurface properties, such as velocity and impedance that are directly interpretable. In contrast, FWI in most published examples is applied only on low-frequency data (typically less than 10 Hz) to enhance the velocity models needed for migration. Brute-force generation of high-resolution subsurface property volumes using FWI can be computationally prohibitive because of the high cost of the required finite-difference simulations. Many of these practical obstacles have been overcome through the use of advanced wave propagation and optimization algorithms and faster computer architectures. In the WBS, detailed subsurface property models generated with FWI have provided an accurate description of the overburden complexity and helped mitigate imaging distortions. The resulting imaging uplift has enabled improved structural definition, stratigraphic characterization of the reservoir, and quantitative interpretation. Predrill predictions using FWI volumes have shown excellent agreement with well results.

Introduction

Romania has a long history of petroleum exploration, with officially registered oil production spanning more than 150 years. While the historic fields are all onshore, exploration activity recently has progressed offshore in the Western Black Sea (WBS). Interest in offshore exploration has increased further in the last few years after ExxonMobil and OMV Petrom drilled the first deepwater hydrocarbon discovery in

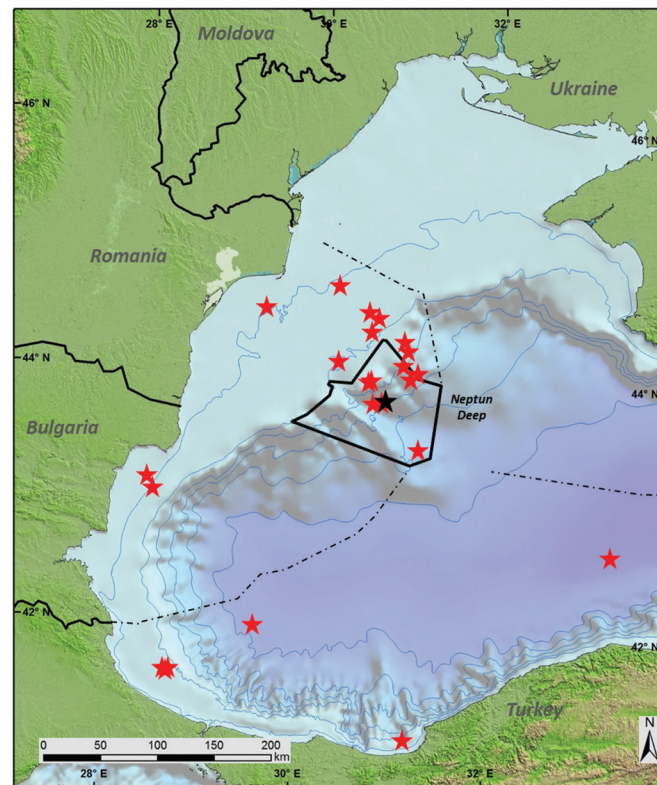


Figure 1. The stars mark the wells drilled in the Western Black Sea since 2011. The Neptun block extent is highlighted in black, and the Domino-1 well is marked with a black star.

the WBS with the 2012 Domino-1 gas well in the Neptun block (see Figure 1).

Several seismic surveys have been acquired over the last decade to support ongoing exploration activity in the WBS. However, seismic imaging in the WBS is very challenging. As illustrated in Figure 2, the presence of complex overburden such as canyons, gas-filled levees, and complex shallow stratigraphy results in distortion of the structure and seismic attributes at the reservoir.

Conventional seismic-imaging technology such as tomography-based velocity model building and seismic migration methods are not adequate to address such challenges due to the small scale of the heterogeneities in the shallow overburden. To overcome the complex seismic-imaging challenges in the WBS and to support the exploration and development program, full-wavefield inversion (FWI) technology was leveraged. A suite of FWI

¹ExxonMobil Upstream Research Company.

²ExxonMobil International Limited.

³ExxonMobil Development Company.

⁴ExxonMobil Exploration Company.

⁵OMV Petrom.

<http://dx.doi.org/10.1190/tle36010060.1>

products has been used to identify shallow hazards, derisk prospects, optimize well placement, perform resource estimation, and support development planning. This article will provide a brief overview of FWI and highlight the key differences between the FWI implementation used for this project and typical implementations in the industry. This article's focus will be on describing the FWI results in the WBS and the impact of these results on exploration activity in the Neptun block.

What is FWI?

The underlying theory for FWI is well known and was first outlined in Tarantola (1984). The goal of FWI is to create a model of the earth's subsurface that fully explains all the seismic wavefields recorded in field seismic data. In contrast, conventional seismic-imaging methods typically utilize only the narrow-angle-reflection part of the recorded seismic wavefields to image the subsurface reflectors.

As illustrated in Figure 3, the FWI method aims to estimate models of subsurface properties so that seismic data simulated in the computer matches the actual field seismic data. The method starts with an approximate initial model of the subsurface

properties. The starting model typically is estimated using conventional methods. For example, tomography is used to estimate a starting model for compressional wave velocity. An accurate full-physics implementation of the wave equation is used to simulate seismic data at all source and receiver locations of the actual field seismic records. The simulated seismic data then are compared to the measured field seismic records, and the mismatch between the simulated and field seismic data is used to update the initial model of subsurface properties. The iterative process of simulating seismic data with updated subsurface property models, comparing with field data, then further updating the subsurface property models using the mismatch between simulated and field data is performed several times until the simulated seismic data matches the field seismic data.

Due to the iterative nature of the FWI method and the computational demands of accurate full-physics simulation, FWI is extremely compute-intensive. In fact, generation of high-resolution subsurface property volumes using full-bandwidth seismic data can be prohibitive because of the high computational requirements of finite-difference simulations necessary to model seismic data. For example, doubling the frequency of simulated seismic data typically requires 16 times more finite-difference computations.

High-resolution FWI workflow for the WBS

In most published examples, FWI is applied on low-frequency diving-wave and refraction seismic data (typically less than 10 Hz) and is used to create an improved (compared to conventional tomography) subsurface velocity model that can enhance seismic migrations. See Warner et al. (2013) for an overview of the technology and practical implementation.

The FWI implementation leveraged for this project has overcome many of the practical computational obstacles to achieving higher resolution (up to 40 Hz) through the use of advanced wave propagation, tuned workflows, optimization algorithms, and faster computer architectures. We use finite-difference-coupled first-order equation in time domain that is second order in time and eighth order in space. Gradients are computed using check pointing as described in Anderson et al. (2012). Lazaratos et al. (2011) and Bansal et al. (2013) describe two of the algorithmic advances that enable high-resolution FWI. In contrast to most published examples of FWI, the FWI implementation used for the WBS provides directly interpretable high-resolution velocity (up to ~15 Hz) and impedance

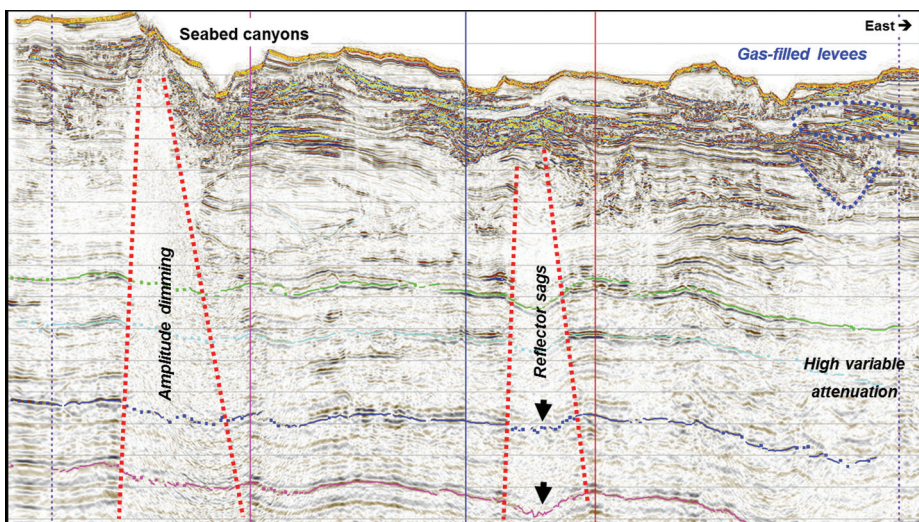


Figure 2. Prestack time-migrated stacked seismic section from the WBS illustrates several seismic-imaging challenges.

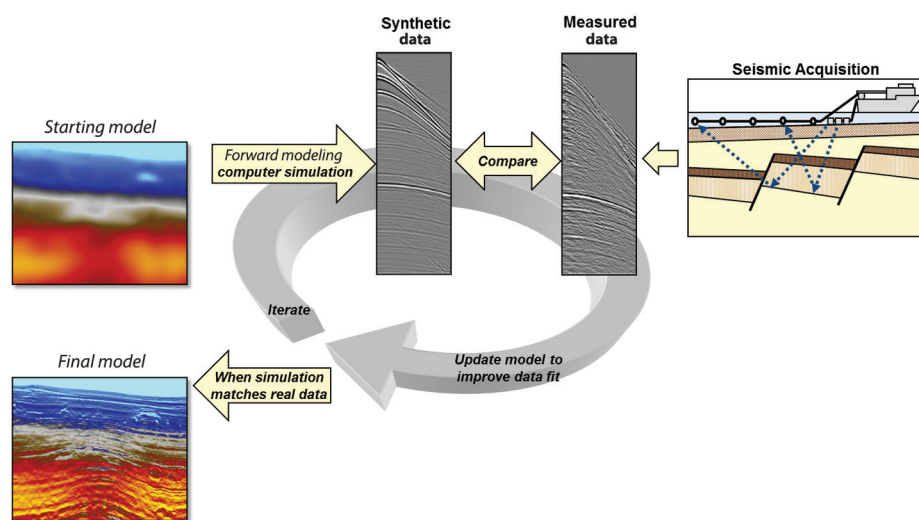


Figure 3. Overview of how FWI works.

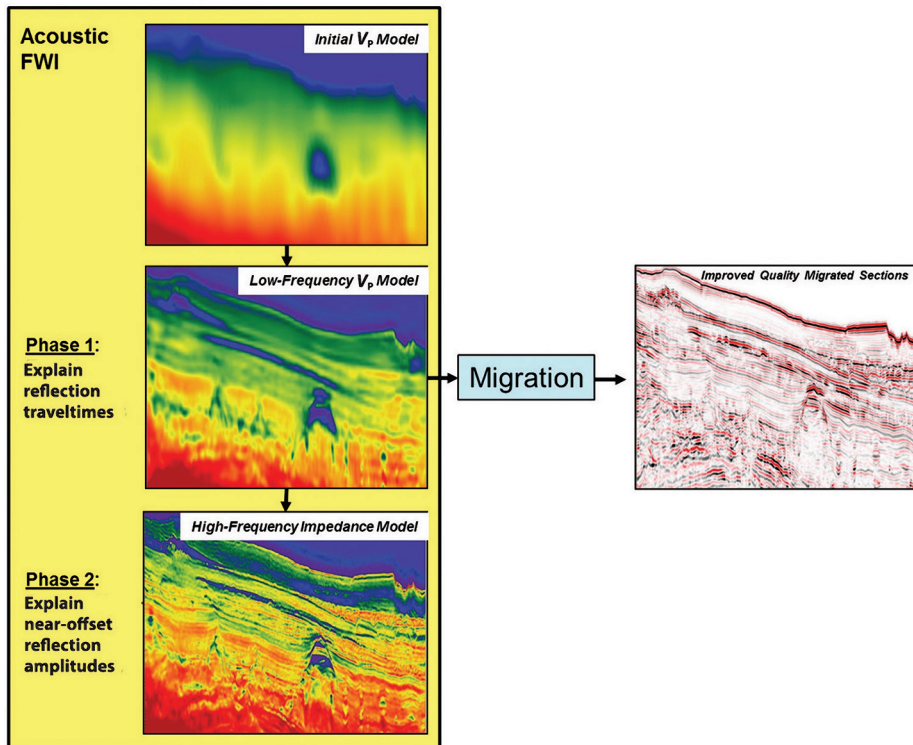


Figure 4. High-resolution FWI workflow in the WBS.

(up to ~40 Hz) volumes in addition to the seismic reflectivity volumes.

Figure 4 illustrates the FWI workflow employed in the WBS. The workflow consists of two stages. The first stage focuses on creating a velocity model that fits the traveltimes or phase information in the reflection data (up to ~15 Hz). The objective function used in the first step is a zero-lag cross correlation (Routh et al., 2011). The FWI velocity results are validated by performing migrations and analyzing improvements in the migration sections. The workflow's second stage focuses on fitting the amplitude information in the reflection data. The velocity model obtained in the first stage is used to construct the initial model for the second stage and then inverted for a high-resolution impedance model that minimizes the amplitude misfit between the simulated data and the measured near-offset data for frequencies up to 40 Hz. The objective function used in the second step is least-squares norm (L2 norm). Further technical details about

the FWI workflow are provided in Lu et al. (2016).

FWI results from the WBS

Figure 5 displays the velocity model obtained with high-effort tomography. This velocity model is relatively smooth (as expected) and served as an initial model for FWI. Figure 6 illustrates that the velocity model updated using FWI provides an obvious resolution improvement compared to tomography and highlights numerous fine-scale velocity features. As shown in Figure 7, the

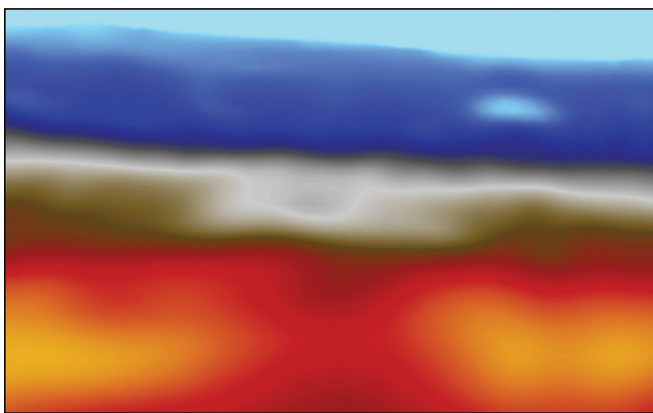


Figure 5. Velocity model obtained using high-effort tomography.

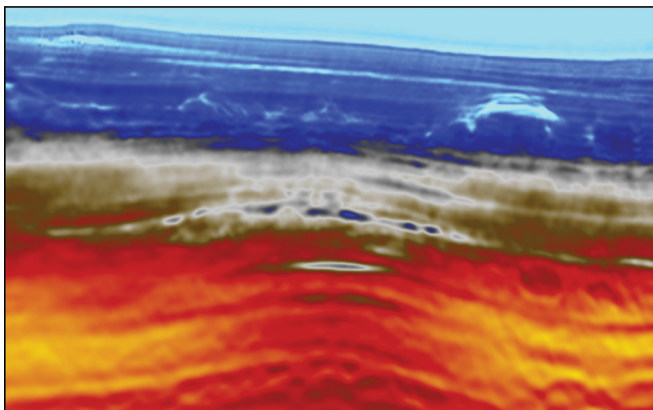


Figure 6. High-resolution (~15 Hz) velocity model obtained using FWI.

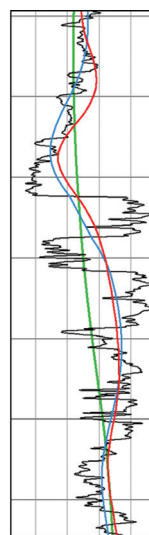


Figure 7. Comparison between measured well sonic velocity, tomography, and FWI velocity. Black = well log sonic; green = tomo velocity; red = FWI velocity; blue = filtered sonic well log.

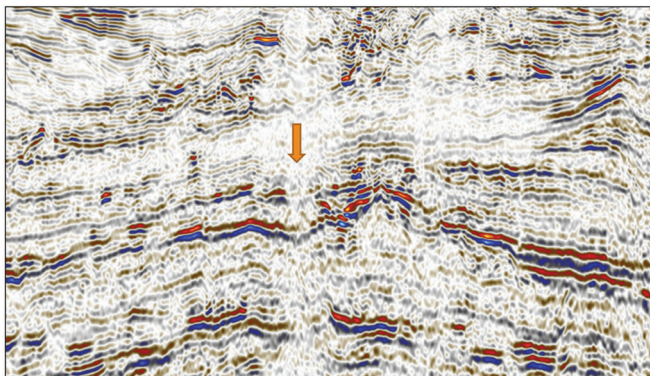


Figure 8. PSDM image with tomography velocity model.

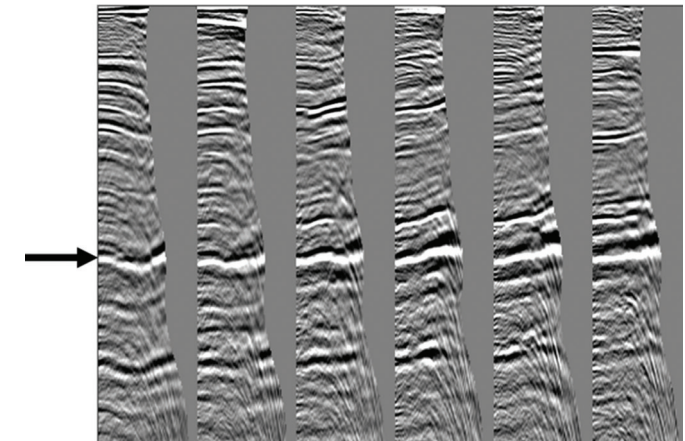


Figure 10. PSDM gathers with tomography velocity model.

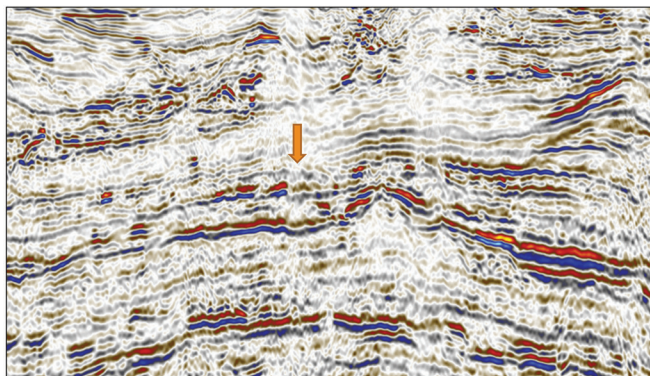


Figure 9. PSDM image with FWI velocity model.

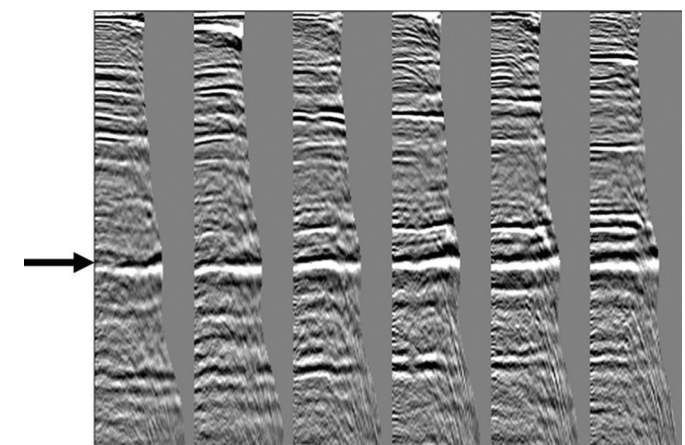


Figure 11. PSDM gathers with FWI velocity model.

estimated FWI velocity demonstrates improved correlation with a well sonic log relative to conventional tomography velocity within the seismic bandwidth.

The accuracy of a velocity model is typically validated by analyzing seismic offset gathers generated by prestack depth migration (PSDM) that utilizes the velocity model as input. The input velocity model for PSDM acts like a lens that focuses the recorded seismic energy to construct the PSDM image. When the velocity model is correct, the seismic reflections are imaged at the same depth across all offsets in a seismic gather (i.e., appear flat in gathers), and reflectors in the stacked PSDM image are well-focused.

Figure 8 shows the seismic image obtained by running PSDM with the smooth tomography velocity model. Since the tomography velocity model does not fully capture the velocity complexity in the shallow overburden, the PSDM image is not well-focused. The arrow in the figure points to a significant structural distortion. Figure 9 illustrates that the PSDM image using the higher resolution FWI velocity model significantly corrects the structural distortions caused by the shallow low-velocity anomalies. Figures 10 and 11 show that the PSDM gathers using the FWI velocity model are flatter than those obtained using the tomography velocity model; the arrows in Figures 10 and 11 point to gathers at a reflector of interest.

The introduction of high-resolution features into the velocity model visually simplifies the seismic image. The clear improvement in the quality of the seismic image along with an improved

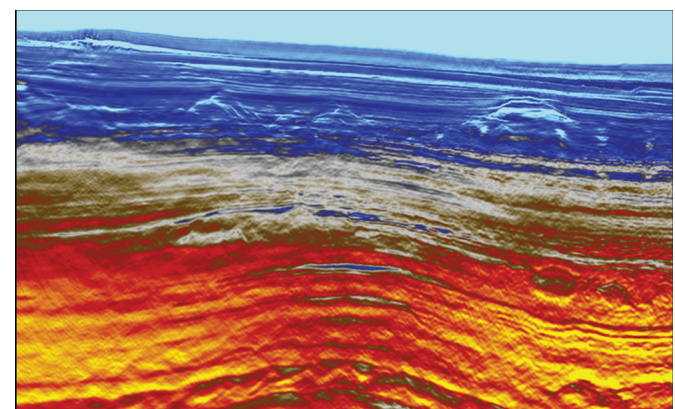


Figure 12. High-resolution (~40 Hz) impedance model obtained using FWI.

match to the well log indicates the accuracy of the estimated FWI velocity model.

Figure 12 shows a cross section from the high-resolution FWI impedance volume obtained from the second stage of the FWI workflow illustrated in Figure 4. This impedance model is obtained by using the FWI velocity model shown in Figure 6 as a starting model and fitting the amplitudes in near-offset seismic data for frequencies up to 40 Hz. The estimated impedance volume can

be utilized for both interpreting the structural and stratigraphic complexities in this field and to extract valuable quantitative information about the subsurface. Figure 13 confirms that the estimated FWI impedance at a well location quantitatively matches the actual measured impedance.

Figures 14 and 15 compare the conventional tomography-based seismic image and FWI velocity-based seismic image from another location in the seismic volume. Note specifically the mitigation of structural sag in Figure 15 compared to Figure 14. Figures 16 and 17 display the FWI velocity and FWI impedance for the same location. These figures illustrate that the high-resolution FWI velocity and impedance volumes can be used for direct quantitative interpretation.

The seismic section illustrated in Figure 17 intersects two recently drilled wells in the WBS. Figures 18 and 19 illustrate a

comparison between FWI's predrill predictions of impedance along the wells versus actual measured impedances. The FWI impedance at both wells matches the actual well-log impedance filtered to seismic resolution remarkably well.

FWI impact

In the WBS, as illustrated in the Results section, detailed subsurface property models generated with FWI have provided a detailed description of the overburden complexity and helped to reduce imaging distortions caused by the overburden. The resulting imaging uplift has enabled improved structural definition of the reservoir. The FWI products also improved our understanding

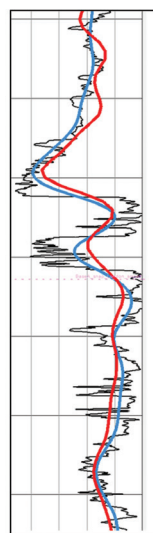


Figure 13. Comparison between measured well-log impedance and FWI impedance. Black = well log; red = FWI impedance; blue = filtered well log.

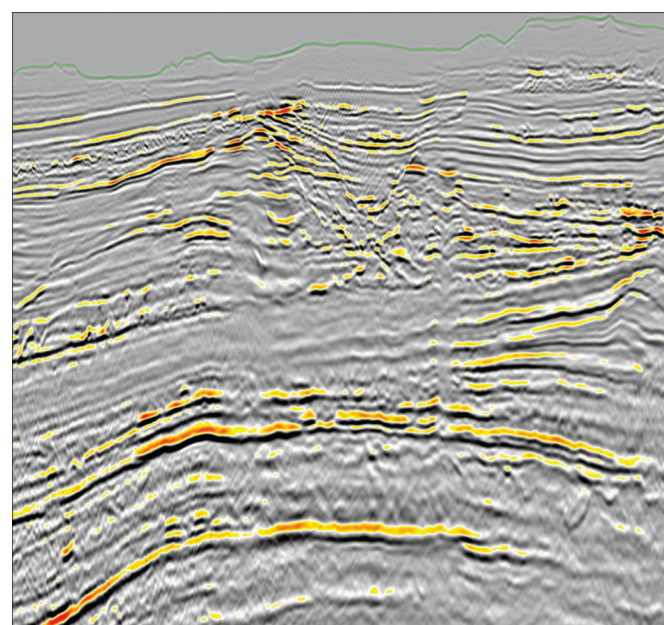


Figure 15. Seismic reflectivity image using FWI velocity model.

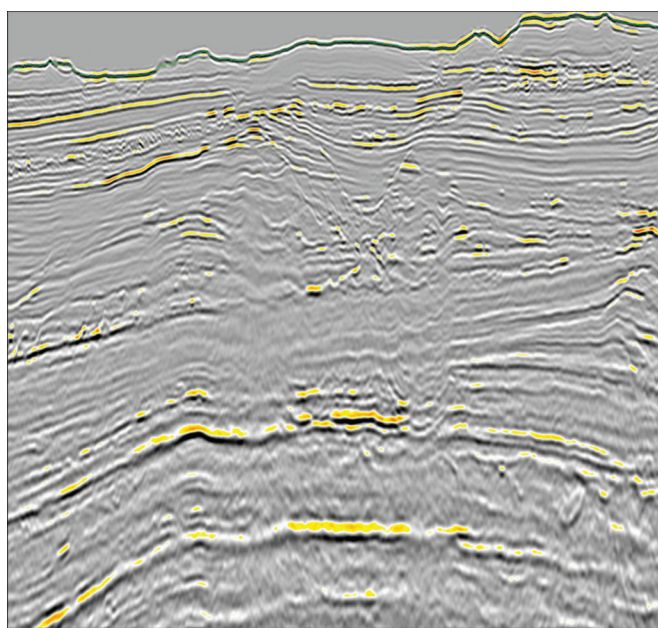


Figure 14. Seismic reflectivity image using tomography velocity model.

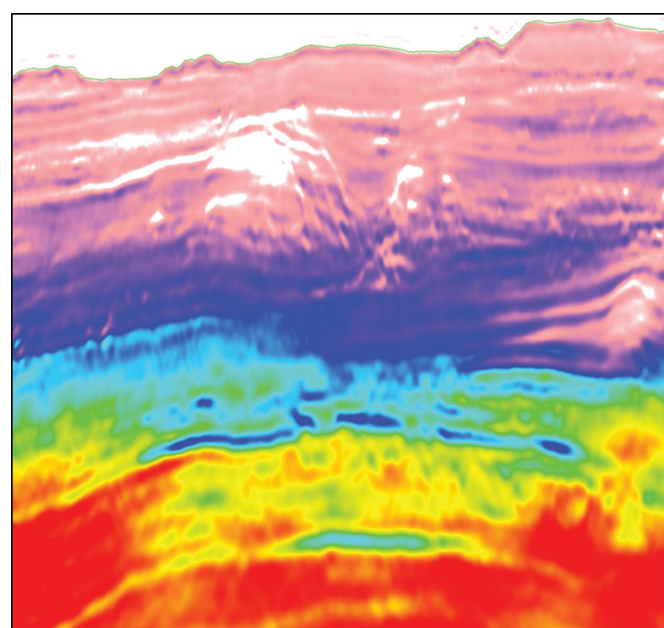


Figure 16. FWI velocity model.

of the environment of deposition and was used in optimizing the locations of two wells (shown in Figures 18 and 19).

The additional information provided by FWI impedance was also used in conjunction with the conventional seismic volumes to provide identification of potential shallow hazards. Figure 20 illustrates the shallow section for one of the recently drilled wells imaged using conventional PSDM and FWI impedance. A low-impedance hazard (Hazard 1 in Figure 20) was transparent in the conventional seismic volume but was clearly visible in the FWI impedance volume, which attests to the fact that FWI has the potential to fill the bandwidth gap typically observed in seismic images. This is discussed in detail in Lu et al. (2016). Improved awareness of the shallow hazards has assisted with successful and safe drilling of wells in the WBS.

The high resolution and quantitative accuracy of the FWI products, confirmed by the successful blind test with the two wells shown in Figures 18 and 19, provide us the confidence to further improve our quantitative understanding of the subsurface lithology and fluid contacts. The FWI volumes enable more confident analysis of the net-to-gross distribution across the field. The volumes are also being used to condition geologic models of the reservoir.

Conclusions

High-resolution FWI represents a step-change in seismic-imaging technology. FWI has both improved our structural understanding of the reservoir units in the Neptun block and provided new perspectives by enabling improved analysis of subsurface properties. **TL**

Acknowledgments

The authors thank the Romanian National Agency of Mineral Resources, OMV Petrom S.A. management, Exxon Mobil

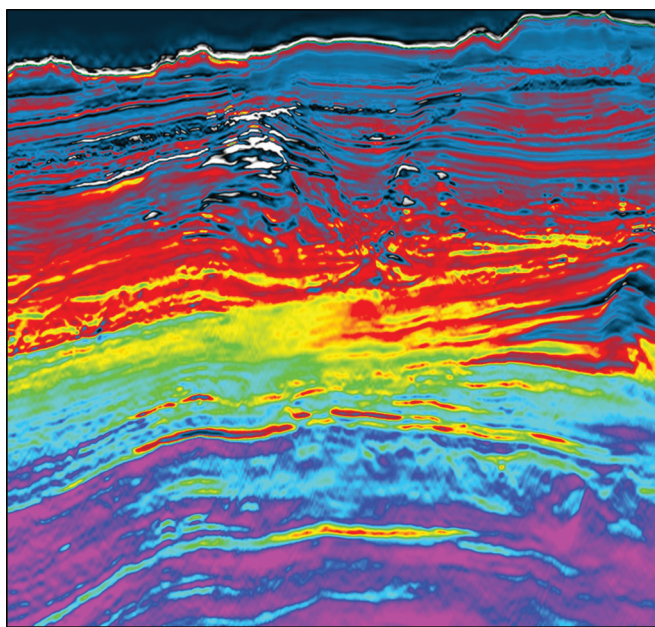


Figure 17. FWI impedance model.

Corporation management, and our colleagues Helen Kallagher and Jake Violet for their discussions and support.

References

- Anderson, J. E., L. Tan, and D. Wang, 2012, Time-reversal checkpointing methods for RTM and FWI: *Geophysics*, **77**, no. 4, S93–S103, <http://dx.doi.org/10.1190/geo2011-0114.1>.
- Bansal, R., J. Krebs, P. Routh, S. Lee, J. Anderson, A. Baumstein, A. Mullur, S. Lazaratos, I. Chikichev, and D. McAdow, 2013, Simultaneous-source full-wavefield inversion: The Leading Edge, **32**, no. 9, 1100–1108, <http://dx.doi.org/10.1190/tle32091100.1>.
- Lazaratos, S., I. Chikichev, and K. Wang, 2011, Improving the convergence rate of full wavefield inversion using spectral shaping: 81st Annual International Meeting, SEG, Expanded Abstracts, 2428–2432, <http://dx.doi.org/10.1190/1.3627696>.
- Lu, R., S. Lazaratos, S. Hughes, and D. Leslie, 2016, Revealing overburden and reservoir complexity with high-resolution FWI:

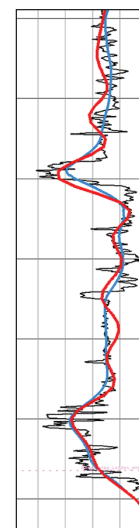


Figure 18. Comparison between predrill FWI impedance prediction and measured well logs for well 1. Black = well log; red = FWI impedance; blue = filtered well log.

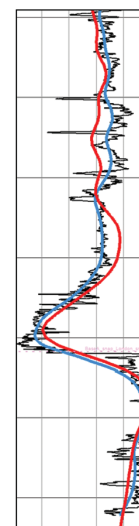


Figure 19. Comparison between predrill FWI impedance prediction and measured well logs for well 2. Black = well log; red = FWI impedance; blue = filtered well log.

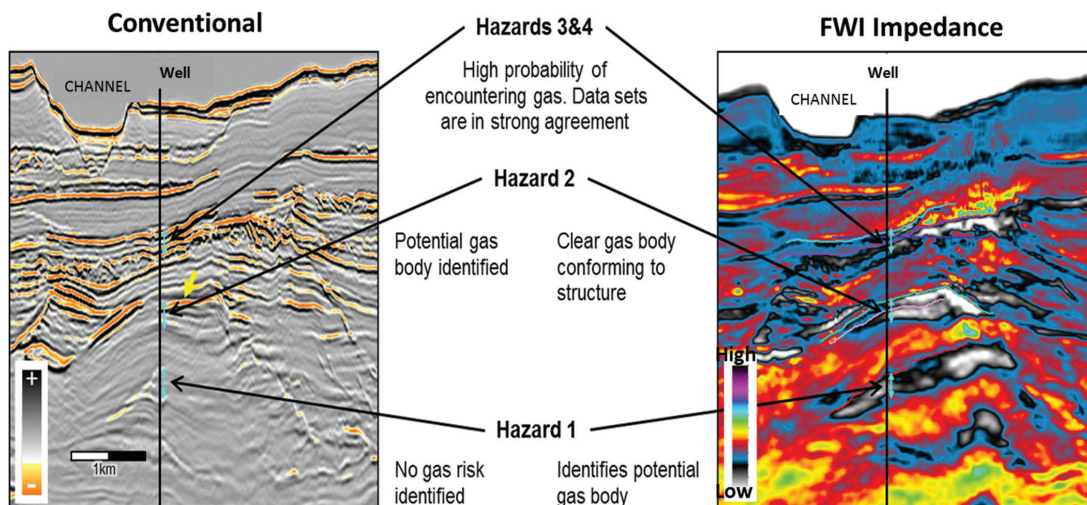


Figure 20. High-resolution FWI impedance (right image) enabled identification of shallow hazards that were not visible on conventional seismic image (left image).

86th Annual International Meeting, SEG, Expanded Abstracts, 1242-1246, <http://dx.doi.org/10.1190/segam2016-13872562.1>. Routh, P., J. Krebs, S. Lazaratos, A. Baumstein, S. Lee, Y. Cha, I. Chikichev, N. Downey, D. Hinkley, and J. Anderson, 2011, Encoded simultaneous source full wavefield inversion for spectrally shaped marine streamer data: 81st Annual International Meeting, SEG, Expanded Abstracts, 2433–2438, <http://dx.doi.org/10.1190/1.3627697>.

Tarantola, A., 1984, Inversion of seismic reflection data in the acoustic approximation: *Geophysics*, **49**, no. 8, 1259–1266, <http://dx.doi.org/10.1190/1.1441754>. Warner, M., A. Ratcliffe, T. Nangoo, J. Morgan, A. Umpleby, N. Shah, V. Vinje, I. Stekl, L. Guasch, C. Win, G. Conroy, and A. Bertrand, 2013, Anisotropic 3D full-waveform inversion: *Geophysics*, **78**, no. 2, R59–R80, <http://dx.doi.org/10.1190/geo2012-0338.1>.